Fisheries Science (2019) 85:943–959
https://doi.org/10.1007/s12562-019-01353-9

ORIGINAL ARTICLE

Biology

Assessing the ability of zebrafish scales to contribute to the short-term homeostatic regulation of [Ca^{2+}] in the extracellular fluid during calcemic challenges

Jacky T. Hung[1] · Sarah E. Webb[1] · Carla Palumbo[2] · Agnieszka M. Lesniak[1] · Alan M. Shipley[3] · Alessandro Rubinacci[4] · Joseph G. Kunkel[5] · Andrew L. Miller[1]

Received: 17 June 2019 / Accepted: 25 August 2019 / Published online: 6 September 2019

Abstract

The elasmoid scales of fish represent a significant internal reservoir of calcium ions (Ca^{2+}), but little is known about the contribution of these scales to the short-term regulation of Ca^{2+} homeostasis in the extracellular fluid (ECF). This gap in our knowledge is partly due to the technical challenges involved in measuring small Ca^{2+} fluxes around the scales of live fish in real time. Here, we describe a technique for exfoliating, mounting, and culturing intact living zebrafish *Danio rerio* scales, then subjecting them to examination using an extracellular, non-invasive, surface-scanning ion-selective electrode technique (SIET). In a Ca^{2+}-sensitive configuration, the SIET can resolve Ca^{2+} flux values in the low-to-sub picomole/square centimeter/second range, with a spatial resolution of approximately 5 µm. We quantified the Ca^{2+} fluxes into and out of scales under different extracellular calcemic challenges set to mimic a variety of Ca^{2+} concentrations in the ECF and showed that the results were similar to those previously reported from isolated mouse metatarsal bone. Our new data extend our current understanding of the role played by fish scales in the short-term homeostatic regulation of Ca^{2+} concentration in the ECF. They also support the suggestion that scales might provide an inexpensive and complementary model for studying the fundamentals of bone-mediated homeostatic Ca^{2+} regulation and the diseases that result from its dysregulation.

Keywords Extracellular fluid Ca^{2+} homeostasis · Scanning ion-selective electrode technique · Zebrafish scales

✉ Andrew L. Miller
almiller@ust.hk

Jacky T. Hung
tshung.wk@gmail.com

Sarah E. Webb
barnie@ust.hk

Carla Palumbo
carla.palumbo@unimore.it

Agnieszka M. Lesniak
alesniak@connect.ust.hk

Alan M. Shipley
amshipley@capecod.net

Alessandro Rubinacci
rubinacci.alessandro@hsr.it

Joseph G. Kunkel
jkunkel1@une.edu

[1] Division of Life Science and State Key Laboratory for Molecular Neuroscience, The Hong Kong University of Science and Technology (HKUST), Hong Kong, China

[2] Section of Human Morphology, Department of Biomedical, Metabolic and Neural Sciences, University of Modena and Reggio Emilia, Modena, Italy

[3] Applicable Electronics, LLC, New Haven, CT, USA

[4] Bone Metabolism Unit, Scientific Institute San Raffaele, Milan, Italy

[5] Pickus Center for Biomedical Research, University of New England, Biddeford, ME, USA

Introduction

There is growing interest in utilizing the zebrafish *Danio rerio* as a complementary model for studying many aspects of mammalian (including human) development, physiology, disease, injury, and regeneration (Dooley and Zon 2000; Ingham 2009; Bakkers 2011; Goldsmith and Jobin 2012; Ablain and Zon 2013; Kalueff et al. 2014; Laizé et al. 2014; Shi et al. 2015; Lin et al. 2016). One topic of ongoing research interest is the ionic homeostasis of body fluids, as well as the conditions and diseases that ensue when this essential regulation is compromised or lost (Hwang and Chou 2013; Guh et al. 2015; Lin and Hwang 2016). One of the ions that plays a key role in this process is the calcium ion (Ca^{2+}) (Blaine et al. 2014; Kwong et al. 2016). Zebrafish (and other fresh-water teleosts) possess an array of complex interacting iono-/osmoregulating mechanisms in various tissues/organs, such as the epithelium, gills, intestines, and kidneys. These control the uptake of Ca^{2+} from the external environment and regulate its concentration inside cells and tissues, as well as in the extracellular fluid (ECF), within strict homeostatic boundaries (Flik and Verbost 1993; Flik et al. 1995; Greenwood et al. 2009; Hwang and Chou 2013). This long-term regulation is achieved in part via a combination of Ca^{2+} sensing elements and systemic hormonal regulation.

In teleosts, including zebrafish, significant internal reservoirs of Ca^{2+} are found in the bones of the endoskeleton and in the elasmoid scales (Waterman 1970; Mugiya and Watabe 1977; Schönbörner et al. 1979; Flik et al. 1986; Rotllant et al. 2005; Sionkowska and Kozlowska 2013). The contribution made by the scales to the long-term regulation of Ca^{2+} homeostasis is well-documented (Takagi et al. 1989; Persson et al. 2000; Rotllant et al. 2005; Metz et al. 2014), and it is known that in times of decreased Ca^{2+} availability (e.g., due to restrictions via the water and/or diet) or increased demand (e.g., during oogenesis and vitellogenesis), Ca^{2+} is preferentially mobilized from scales rather than from the bones (Mugiya and Watabe 1977; Takagi et al. 1989; Persson et al. 1998; Metz et al. 2014). However, little is known about the possible role played by the scales in the short-term, minute-to-minute homeostatic regulation of Ca^{2+}, such as that attributed to the bones in mammals (Marenzana et al. 2005; Dedic et al. 2018; Hohman et al. 2018). This gap in our knowledge is partly due to the technical challenges involved in detecting and measuring the diminutive Ca^{2+} fluxes around the scales of live fish in real time while subjecting them to various calcemic challenges and/or when under the influence of various systemic Ca^{2+} regulators. However, in the study reported here we exfoliated and cultured living scales from zebrafish (Sire et al. 2000; Pasqualetti et al. 2012a; Metz et al. 2014; Fig. 1) and then used a non-invasive, extracellular, scanning Ca^{2+}-sensitive microelectrode (Fig. 2) to measure Ca^{2+} fluxes into and out of both sides of the scales under different extracellular calcemic challenges set to mimic a variety of Ca^{2+} concentrations ($[Ca^{2+}]$) in the ECF (Kühtreiber and Jaffe 1990; Smith et al. 1999; Marenzana et al. 2005; Dedic et al. 2018).

Like bone, zebrafish scales contain mineralized hydroxyapatite and collagen-based matrix components (Waterman 1970; Sire et al. 1997; Sire and Akimenko 2004; Ogawa et al. 2010; De Vrieze et al. 2011), as well as populations of different cell types that play a key role in their development, maintenance, regeneration, and physiology (Sire et al. 2000; Pasqualetti et al. 2012a; Metz et al. 2014; Iwasaki et al. 2018; Fig. 1a, b). The hyposquamal (innermost) side of the scale consists of a layer of incompletely mineralized tissue, which is mainly composed of several layers of collagen fibrils organized into a plywood-like structure (Sire et al. 1997; Sire and Akimenko 2004; Pasqualetti et al. 2012b; Fig. 1b). In contrast, the episquamal (outermost) side of the scale has a thin layer of highly mineralized (hydroxyapatite-rich) tissue that comprises a network of interwoven collagen fibrils (Meunier 1984; Sire and Akimenko 2004; Fig. 1b). In addition, the episquamal surface displays distinct features in the form of concentric hydroxyapatite ridges called circuli, as well as grooves (called radii) that fan-out from the anteriorly-located scale focus (Pasqualetti et al. 2012a; Fig. 1b, ci). This surface topography has a significant influence on the morphology, distribution, and type of cells residing on this surface (Pasqualetti et al. 2012a, b). In contrast, the surface of the hyposquamal side is quite smooth and relatively featureless (Pasqualetti et al. 2012b), and it displays cells with a different morphology and distribution to those on the episquamal surface (Fig. 1b, cii).

Here, we report for the first time that exfoliated zebrafish scales can independently detect and respond to changes in $[Ca^{2+}]$ in their bathing medium and that they do so on a short-term (i.e., minute-to-minute) basis. Thus, our data indicate that scales show a similar short-term Ca^{2+}-related homeostatic activity to that previously reported for mammalian bone (Marenzana et al. 2005; Dedic et al. 2018).

Materials and methods

Zebrafish husbandry

The AB wild-type zebrafish line was maintained at approximately 28.5 °C on a 14-h light/10-h dark cycle (Westerfield 2000) in the HKUST Zebrafish Facility. AB fish were obtained from the Zebrafish International Resource Center (ZIRC; University of Oregon, Eugene, OR, USA). All procedures used in this study with live fish were performed in

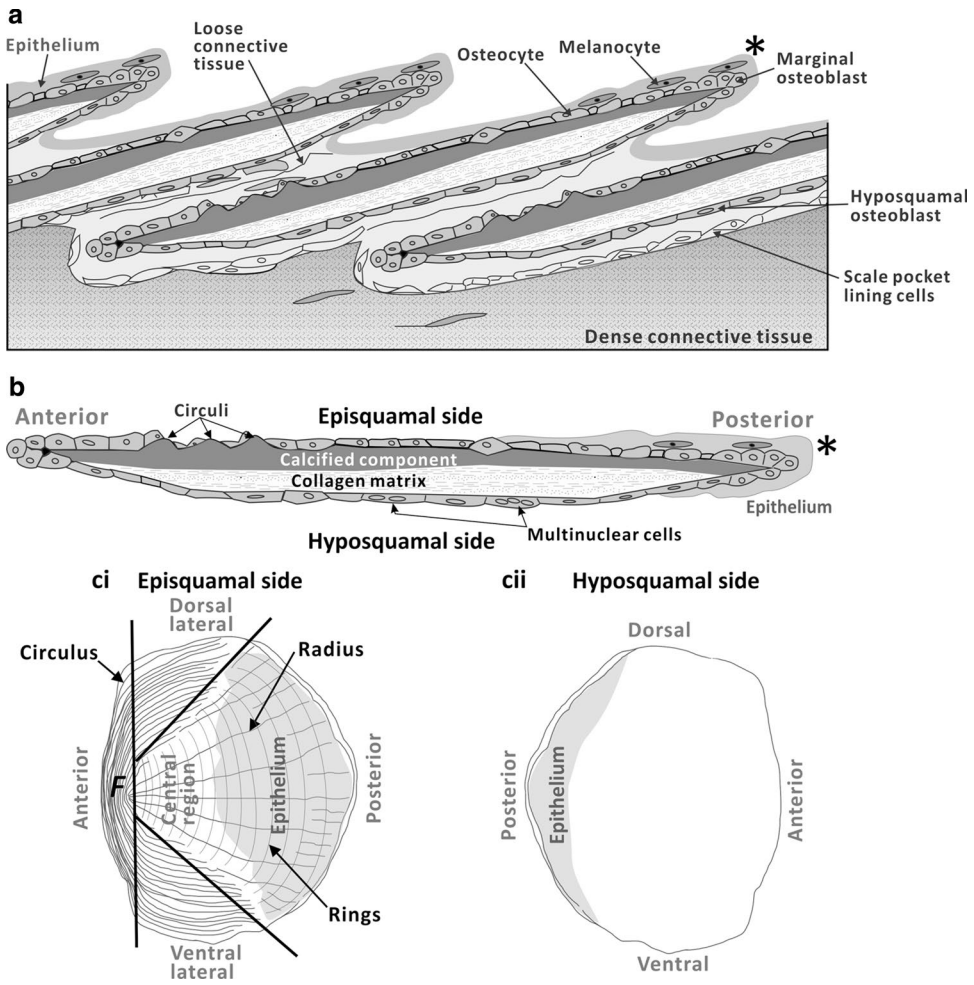

Fig. 1 Schematic illustrations showing the morphology of the zebrafish *Danio rerio* scale. **a** The typical arrangement of scales in the zebrafish trunk. This is a sagittal section showing the scales and the surrounding cells and tissues. The asterisk indicates the posterior end of a scale, as shown in **b**. **b** Side-view of a scale that has been exfoliated from the trunk of a zebrafish. **c** The main morphological features on the episquamal (**ci**) and hyposquamal (**ci**) sides of a scale. *F* indicates the location of the scale focus. Images are not drawn to scale. Panel **a** is modified from Elliott (2000)

accordance with the guidelines and regulations set out by the Animal Ethics Committee of the HKUST and by the Department of Health, Hong Kong.

Preparation of the scanning ion-selective electrode technique-compatible scale bathing medium

Scale bathing medium was a modified version of a medium originally developed for culturing fish hearts (Burns and MacRae 2006). It consisted of solutions A and B. The components, concentrations, and osmotic coefficients of solution A (1× dilution) are listed in Table 1. It was initially prepared as a 12.5× stock solution in Milli-Q water, after which it was filtered through a 0.22-μm filter (SCGPU10RE; EMD Millipore Corp., Billerica, MA, USA) and stored at 4 °C until required (or for a maximum of 30 days). Solution B was simply $CaCl_2$ (osmotic coefficient 0.9621; Pan 1977), which was prepared as a 100× stock at three concentrations (1, 150, and 300 mM) and then stored at room temperature. To prepare the 1× scale bathing medium, we mixed 40 ml stock solution A, 5 ml stock solution B, and 1.134 g (27 mM) $NaHCO_3$ in Milli-Q water to give a final volume of 500 ml; this medium was stored at 4 °C until required (or for up to 1 week). For each batch of 1× scale bathing medium prepared, a sample was tested with an osmometer (model 3320; Advanced Instruments, Inc., Norwood, MA, USA) and a pH meter to ensure that an osmolarity of approximately 290 ± 10 mOsm/kg and a pH of 7.35 were maintained.

Exfoliation of zebrafish scales

Scales were obtained from an approximately 1-year-old adult AB fish. Prior to scale exfoliation, fish were anesthetized using a chilling protocol, as described previously (Kinkel et al. 2010). The anesthetized fish were then transferred to a cold 60-mm glass Petri dish lid for scale removal. Scale removal was performed using a pair of no. 5 watchmaker's forceps (Regine Switzerland SA, Morbio Inferiore, Switzerland) while viewing the fish under a stereomicroscope. A scale with its connected epidermal layer (in the posterior region; Fig. 1) was gently removed from the body of the fish and bathed in scanning ion-selective electrode technique (SIET)-compatible scale

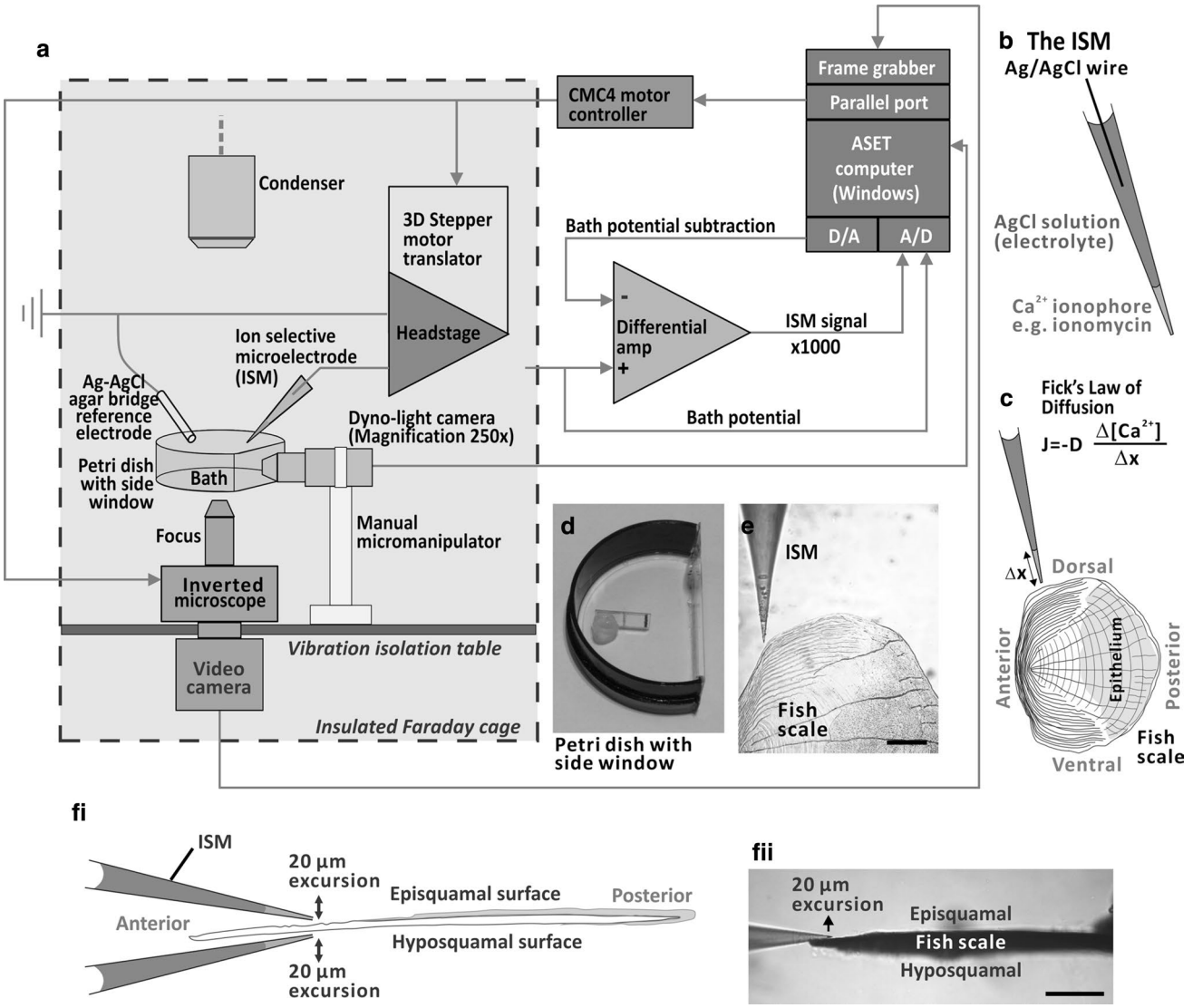

Fig. 2 The scanning ion-selective electrode technique (SIET). **a** Schematic of the SIET system. **b** The ion-selective microelectrode (*ISM*). **c** The ISM was oscillated over a distance of Δx from the scale, and the difference in voltage measured between the two points was then used to calculate the ion flux rate via Fick's law of diffusion, as shown by the equation, such that J is the calcium ion (Ca^{2+}) flux in the x direction, $\Delta[Ca^{2+}]/\Delta x$ is the Ca^{2+} concentration gradient, and D is the diffusion constant of Ca^{2+}. **d** The custom-made measuring chamber prepared from a Petri dish with a glass side-window. **e** A zebrafish scale that is being scanned by the ISM. **f** Schematic (**fi**) and photomicrograph (**fii**) to shown the side view of a scale and the 20-µm excursion step used to scan the episquamal and hyposquamal surfaces. Scale bars (**e**, **fii**): 200 µm. *ASET* Automated scanning electrode technique. **a** Modified from Fig. 2 in the scanning microelectrode techniques (SIET/SPET) system manual (Shipley 2009)

culture medium. After scale exfoliation, the donor fish was placed in a recovery tank before being returned to the fish facility. Only scales removed from row C, positions I, II, III, IV, and V (Sire et al. 2000) were used in these experiments, as these are flatter than those removed from the other rows and are thus better suited to SIET-based examination.

Scanning ion-selective electrode technique

Non-invasive measurement of real-time Ca^{2+} fluxes (pmol/cm^2/s) in the extracellular medium adjacent to the surface of zebrafish scales was accomplished using the SIET (Fig. 2; Applicable Electronics LLC, New Haven, CT, USA). This technique has been utilized extensively over the past 25 years

Table 1 Composition of stock solution A of the scale bathing medium (at 1× dilution) and the osmolarity coefficient of each component

Chemical	Concentration (mM)	Osmotic coefficient φ
NaCl	136.90	0.933[a]
KCl	5.37	0.940[a]
$MgCl_2$	0.98	0.963[b]
$MgSO_4$	0.81	0.901[c]
KH_2PO_4	0.44	0.988[a]
Na_2HPO_4	1.71	0.542[d]
D-Galactose	5	1.061[e]
HEPES	5	–
$NaHCO_3$	27	0.883[f]
Theoretical osmolarity (mOsm/kg)	338.04	

[a]Hamer and Wu (1972)

[b]Goldberg and Nuttall (1978)

[c]Rard and Miller (1981)

[d]Goldberg (1981)

[e]Catté et al. (1995)

[f]Pitzer and Peiper (1979)

(Kühtreiber and Jaffe 1990; Smith et al. 1999; Kunkel et al. 2006; Reid and Zhao 2011) to measure the free-ion concentration gradients of specific ions (in our case, Ca^{2+}) by means of a single ion-sensitive microelectrode (ISM in Fig. 2a, b) that is repeatedly moved between two measuring positions using a system of stepper motors at a selected distance (i.e., 20 µm; Fig. 2c, e, fi, fii) and at programmed repetition rates of < 1 Hz (typically in the range of approx. 0.3–0.5 Hz) to minimize mixing of the scale bathing medium. The ISM was controlled using a computer via an automated scanning electrode technique (ASET) program (Applicable Electronics LLC; Fig. 2a). Thus, positioning of the ISM around the scale at the measuring and reference positions and control of the stepping excursion and sampling times were all software programmable. The ISM records a voltage (representing the local [Ca^{2+}]) at each measuring point. Baseline or reference measurements were taken a few millimeters away from the scale, where no Ca^{2+} gradient was detected. All measurements at the scale surface were compared to reference readings taken periodically during the experiment. Each gradient data point was calculated by subtracting the [Ca^{2+}] values measured at each position. The Ca^{2+} flux was derived from Fick's law of diffusion: $J = -D(\Delta[Ca^{2+}]/\Delta x)$, where J is the Ca^{2+} flux in the x direction, $\Delta[Ca^{2+}]/\Delta x$ is the Ca^{2+} concentration gradient, and D is the diffusion constant of Ca^{2+} (Fig. 2c).

ISMs were fabricated from borosilicate glass capillaries with an outer diameter of 1.5 mm (TW150-4; World Precision Instruments Inc., Sarasota, FL, USA). The capillaries were pulled in two stages (to achieve an approx. 3- to 5-µm-diameter tip; Fig. 2e, fii) on a Flaming Brown Model P-97 electrode puller (Sutter Instruments, Novato, CA, USA), after which their inner surface was coated with vaporized hydrophobic silane (*N*,*N*-dimethyltrimethylsilylamine) in a dedicated oven (Heratherm OGS60; Thermo Fisher Scientific, Waltham, MA, USA) at 200 °C (Smith et al. 1999). The ISMs were then backfilled with 100 mM $CaCl_2$ electrolyte to a column length of approximately 1 cm, and then front-loaded with an approximately 30- to 40-µm-long column of a liquid Ca^{2+} ion exchanger (Ca^{2+} Ionophore 1, cocktail A; Fluka Chemie AG, Buchs, Switzerland). An ISM was then connected to an ion head-stage amplifier (Applicable Electronics LLC) via a short piece of silver chloride-plated silver (Ag/AgCl) wire. This assembly acted as the measuring ISM (Fig. 2b). A new ISM was made for each experiment. The reference electrode was an Ag/AgCl half-cell (MEH3S; World Precision Instruments, LLC, Sarasota, FL, USA), connected to the scale bathing medium (or calibration solution) by a PVC capillary tube filled with 3 M KCl and 0.5% agar. Before each experiment the ISM was calibrated against a series of Ca^{2+}-containing test solutions (i.e., containing 0.1, 1.0, or 10.0 mM $CaCl_2$). ISMs with a deviation in their Nernst Slope of > 3 mV from the theoretical value (i.e., between 27 to 33 mV) were discarded and a new ISM fabricated. With appropriate shielding and grounding, the SIET has been reported to resolve Ca^{2+} flux values in the low-to-sub picomole/square centimeter/second (pmol/cm^2/s) range (Kühtreiber and Jaffe 1990). The tip diameter of the ISM determines the spatial resolution of the technique. We were able to pull tips that were approximately 3–5 µm in diameter, and this represents the resolution we achieved during this study. This resolution allowed us to identify the specific scale surface regions generating the inward and outward Ca^{2+} fluxes.

Scale mounting and SIET-based data acquisition

For Ca^{2+} fluxes to be measured at various positions on both sides of the zebrafish scale, the fragile tip of the ISM had to be positioned very carefully and accurately close (i.e., within a distance of approx. 5 µm) to the scale surface. To achieve this, a bottom- and side-viewing scale measuring chamber was designed (Fig. 2d). Scales located in the measuring chamber were then visualized simultaneously from the bottom and the side using a Zeiss Axiovert-100 inverted microscope (Carl Zeiss GmbH, Oberkochen, Germany) equipped with FLUAR 2.5X/0.12 NA and Plan-APOCHROME 10 ×/0.32 NA PH1 objective lenses (Carl Zeiss GmbH), and a USB CMOS camera (Ui-1640LE; IDS Imaging Development Systems GmbH, Obersulum, Germany) for the former, and a Fluor USB Dino-Lite side-mounted microscope

(AnMo Electronics Corporation, Hsinchu, Taiwan) for the latter (Fig. 2a). Both microscopes were mounted on a vibration isolation table (Technical Manufacturing Corp., Peabody, MA, USA). The Dino-Lite microscope was mounted via a manual manipulator (MM-33N; Narishige, Tokyo, Japan) using an HD-M1 Dino-Lite mount (AnMo Electronic Corp.). The Dino-Lite microscope was adjusted to a magnification of ×250 and calibrated using a grating provided by the manufacturer. The entire isolation table, microscope, and head-stage electronics were mounted within an insulated Faraday cage (Fig. 2a). For all the SIET-based experiments, the environment within the Faraday cage was maintained at approximately 28.5 °C with a heating system and controller unit custom-built by the Electrical and Mechanical Fabrication Unit of the Design and Manufacturing Services Facility at the HKUST.

The bottom- and side-viewing scale measuring chambers were made from a 35-mm Petri dish (Falcon, Becton, Dickinson and Company, Franklin Lakes, NJ, USA), which had a section cut out of it using a hot razor blade, after which the cut edges were smoothed down to achieve a flat surface (Fig. 2d). A 1.2 × 3.6-cm piece of cover glass (no. 1.5) was affixed to the cut surface using high vacuum grease (Dow Corning Corp., Midland, MI, USA) to produce an optically clear side-viewing window for the Dino-Lite microscope. An acrylic block of approximately 15 × 15 × 3 mm featuring a 0.7-mm slit halfway along the length of one side was affixed to the inner surface of the measuring chamber using high vacuum grease. Exfoliated scales were sandwiched at their posterior edges between two pieces of plastic film, and this film was then inserted into the slit in the acrylic block to immobilize the scale. Depending on the orientation of the acrylic block, the scale could be presented in either a vertical or horizontal orientation for subsequent SIET-based examination (Fig. 2d). The ISM was vibrated orthogonal to the surface of the scale, with a 20-µm excursion (vibration amplitude) for all experiments. The closest point to the scale surface was set at 5 µm.

In one series of SIET-based experiments, scales were sequentially exposed to three different solutions of scale bathing medium supplemented with 0.01 (hypocalcemic), 1.5 (isocalcemic), or 3.0 mM (hypercalcemic) $CaCl_2$ in order to present the scale with a series of immediate calcemic challenges in the absence of any systemic regulatory hormones. At each $[Ca^{2+}]_{ext}$ used (beginning with 0.01 mM $CaCl_2$), measurements were initially made at a background measuring position (approx. 5 mm away from the scale surface) for 3 min to ensure a stable baseline signal from the calibrated ISM. Following this, measurements were made at three positions of the scale (i.e., dorsal, ventral, and anterior), at approximately 5 µm from the scale surface on the episquamal side (spending approx. 3 min at each measuring site). This was then followed by a similar procedure on the hyposquamal side (Fig. 2e, fi, fii). The ISM was then returned to the background measuring position for 1 min to assess its performance and stability. The scale bathing medium was then changed to one containing 1.5 mM $CaCl_2$ (considered to be isocalcemic with the reported $[Ca^{2+}]$ of zebrafish blood serum; Nakari and Erkomaa 2003). This was done by the repetitive (i.e., ≥ 3 times) removal and addition of new medium (using a P-200 pipette tip attached to a 10-ml Luer lock-tip syringe; SS0114H29; Muzamal Industries, Cheras, Malaysia) in order to ensure complete medium replacement. The scan protocol described above was repeated with medium containing 1.5 mM $CaCl_2$, and then with medium containing 3.0 mM $CaCl_2$. No SIET measurements were made in the posterior region of scales due to the presence of remnants of the epithelial layer covering this region of the scale following exfoliation.

In vitro labeling of scales with SYTO 11 and SYTOX orange nucleic acid stains

To test the viability of the scale cells during the time window that the SIET experiments were carried out, we conducted a second series of experiments in which scales were bathed in SYTO 11 live-cell nucleic acid stain and SYTOX orange nucleic acid stain (S-7573 and S-11368, respectively; Molecular Probes™, Thermo Fisher Scientific, Inc.). SYTOX orange nucleic acid stain is membrane impermeable and so only labels dead cells. The scales were removed from AB strain male zebrafish as described previously and then incubated in measuring medium containing Ca^{2+} at 0.01, 1.5, or 3 mM ($n = 4$ for each treatment). The scales were collected and bathed in SIET measuring medium for different periods of time (i.e., 0.5, 1, 2, 4 h), after which they were transferred to measuring medium containing 0.5 µM SYTO 11 and 5 µM SYTOX orange in the dark for 20 min. The scales were then washed with phosphate buffered saline (PBS) prior to fixation with PBS containing 4% paraformaldehyde (Electron Microscopy Sciences, Hatfield, PA, USA) for 30 min in the dark. The samples were subsequently washed in PBS for 3 × 5 min and mounted under Prolong® Gold antifade mountant (P-36930; Molecular Probes™, Thermo Fisher Scientific, Inc.). The mountant was allowed to cure in the dark at room temperature for 24 h before the labeled scales were imaged using a Leica TCS SP5 II laser scanning confocal microscope (Leica Microsystems GmbH) with a DMI 6000 motorized stage (Leica Microsystems GmbH) using an HC PL APO 20 ×/0.7 NA lens. All images were collected at a resolution of 1024 × 1024 pixels and a confocal scan speed of 100 Hz with 3× frame signal averaging. SYTO 11 and SYTOX orange fluorescence was visualized using simultaneous excitation with an Argon laser at 476 nm and a DPSS laser at 561 nm, respectively, and at detection ranges of 482–543 and 566–605 nm, respectively.

Images were captured with the Leica LAS AF software and analyzed with NIH ImageJ (Schneider et al. 2012) or DotCount (ver. 1.2.1; Reuter 2012) for cell counting purposes. The images were then arranged with CorelDraw X6 (Corel Corp., Ottawa, ON, Canada).

Biotic determination of the Ca^{2+} fluxes detected by the SIET

Experiments were conducted to determine if the Ca^{2+} fluxes generated around intact zebrafish scales under various calcemic challenges were biotic in nature. In the first series of experiments, exfoliated scales were first killed by air drying for 2 days and then rehydrated for 3 days at 4 °C in bathing medium supplemented with 0.01, 1.5, or 3.0 mM $CaCl_2$. The scales were then slowly warmed to approximately 28.5 °C prior to SIET-based examination, which was conducted as described previously. In these experiments, measurements were made on both the episquamal and hyposquamal sides of scales but just in the dorsal quadrant. In the second series of experiments, exfoliated scales were killed by treatment with potassium cyanide (KCN). In these experiments, measurements were made before and after the addition of KCN (to a final dish concentration of 10 mM) on the episquamal side of exfoliated scales in medium supplemented with 0.01 mM $CaCl_2$.

Statistical analysis

Numerical data were exported to Minitab 17.3.1 (Minitab, LLC, State College, PA, USA) for statistical analysis. For multiple comparisons, sets of data were initially screened with one- or two-way analysis of variance, followed by Tukey–Kramer test to determine which pairs of means were significantly different from each other. When comparing just two sets of data, the Student's *t* test was used.

In vivo and in vitro labeling of scales with alizarin red S

The localization of Ca^{2+} in zebrafish scales was detected using both live staining and post-fixation staining protocols. In the former, adult zebrafish were maintained in fish water (1 fish per 500 ml) containing 10 mM HEPES and 50 µg/ml alizarin red S dye (both from Sigma-Aldrich Co. LLC, St. Louis, MO, USA) at pH 7.2 and approximately 28.5 °C in the dark overnight. The fish water consisted of deionized water containing 88 mg/l Instant Ocean sea salt (Aquarium Systems, Sarrebourg, France) and 0.6 mg/l $NaHCO_3$ (Sigma-Aldrich Co. LLC); the latter was used to adjust the pH of the water. After staining, the fish were transferred to clean fish water at approximately 28.5 °C in the dark for approximately 5 min to remove excess alizarin red S from the body. The fish were anaesthetized in 0.02% buffered MS-222 solution (comprising 0.65 mM MS-222 and 0.8 mM Tris-base, pH 7.2; both Sigma-Aldrich Co. LLC) at room temperature, and several scales were removed. The fish were then allowed to recover in clean fish water.

For in vitro labeling, zebrafish were anaesthetized in MS-222 at room temperature and scales were removed. The samples were then fixed with PBS containing 4% paraformaldehyde solution for 30 min at room temperature, after which they were washed with PBS. The fixed scales were then incubated with PBS containing 0.5 mg/ml alizarin red S in the dark for 1 h. After staining, the scales were mounted with deionized water containing 70% glycerol or were processed for cryosectioning.

For cryosectioning, scales were embedded in PBS containing 5% sucrose and 1% agarose. The agarose blocks were trimmed to align the samples orthogonally to the cut face for subsequent cryosectioning. The trimmed blocks were then immersed in PBS containing 30% sucrose overnight, after which they were transferred to a plastic mould (Electron Microscopy Sciences) and embedded in Tissue-Tek OCT compound (Sakura Finetek Japan Co. Ltd., Tokyo, Japan). The orientation of individual specimens was adjusted, after which they were frozen at − 23 °C for at least 30 min prior to cryosectioning. After the sample and embedding medium were frozen solid, they were removed from the mould and mounted into a specimen holder in a CryoStar NX70 cryostat (Thermo Fisher Scientific Inc.). Sections 30 µm thick were prepared and mounted on Superfrost plus adhesion slides (Thermo Fisher Scientific Inc.) and mounted under Prolong Gold antifade mountant (Molecular Probes™).

Epifluorescence images were acquired using a Nikon Digital Sight cooled colour matrix CCD camera (DS-5Mc; Nikon Corp., Tokyo, Japan) mounted via a 0.6× adaptor to a Nikon AZ-100 M stereomicroscope using an AZ Plan Apo 4 ×/0.4 NA objective lens and a G-2A filter block. The visualization of alizarin red S fluorescence was achieved using a 510- to 560-nm band-pass excitation source and a 575-nm long-pass emission filter. Bright-field images of the scale samples were collected using the same microscope system with a Fiber Illuminator (C-FI115/230; Nikon Corp.), and the Nikon NIS Elements Advanced Research imaging software (version 3.22.00; Nikon Corp.) was used to capture and export images.

Electron microscopy examination

At the end of some of the SIET-based experiments, scales were fixed for 1 h with 4% paraformaldehyde in 0.13 M phosphate buffer (pH 7.4); post-fixed for 1 h with 1% osmium tetroxide in 0.13 M phosphate buffer (pH 7.4); dehydrated in graded ethanol; embedded in epoxy resin (Durcupan ACM; Electron Microscopy Sciences); then

sectioned with a diamond knife mounted in an Ultracut microtome (Reichert-Jung, Wetzlar, Germany). Ultrathin Sections (70–80 nm) were mounted on formvar- and carbon-coated copper grids, stained with 1% uranyl acetate and lead citrate, and then examined under a Zeiss EM109 transmission electron microscope (Zeiss AG, Jena, Germany).

Results

Ca^{2+} fluxes generated by the cells of intact scales in culture when challenged by different [Ca^{2+}] in the measuring media ($[Ca^{2+}]_{ext}$)

The SIET was used to measure real-time Ca^{2+} fluxes into and out of scale tissue as a read-out of absorption (influx of Ca^{2+} into the scale) or mobilization (efflux of Ca^{2+} from the scale), respectively. Scales were bathed in measuring media containing three different [Ca^{2+}]: 1.5 mM (isocalcemic $[Ca^{2+}]_{ext.}$), to mimic the normal (physiological) Ca^{2+} concentration in the plasma of male adult zebrafish (Nakari and Erkomaa 2003); 0.01 mM (hypocalcemic $[Ca^{2+}]_{ext.}$); or 3 mM (hypercalcemic $[Ca^{2+}]_{ext.}$). They were scanned at three different locations (dorsal, ventral, and anterior) on the episquamal, and hyposquamal surfaces of scales (Fig. 3ai, aii) in order to determine which surface and which locations were responsible for generating Ca^{2+} fluxes under different calcemic challenges. Intact scales ($n = 5$ for each experiment) were mounted in measuring chambers and subjected to sequential scanning at the three different concentrations of Ca^{2+} in the bathing medium (starting with the lowest) over a period of approximately 50 min for each experiment. This time-frame included moving the probe between the reference and measuring positions and changing the bathing medium. For each of the regions and $[Ca^{2+}]_{ext}$ being tested, the Ca^{2+} flux values measured at the scale surface were averaged over a period of 5 min. Figure 3bi–biii display three bar graphs showing the mean ± standard error of the mean (SEM) of Ca^{2+} flux values generated by intact zebrafish scales in measuring media containing 0.01, 1.5, and 3.0 mM Ca^{2+}, respectively. As predicted, under isocalcemic conditions (i.e., 1.5 mM Ca^{2+}), relatively little movement of Ca^{2+} was recorded in either direction (influx or efflux). However, under hypocalcemic conditions (i.e., in 0.01 mM Ca^{2+}), a significant (at $P < 0.05$) efflux of Ca^{2+} was recorded at every measuring position (dorsal, anterior, and ventral) on the episquamal side of the scale, when compared with the fluxes observed under isocalcemic conditions. Small effluxes were also observed on the hyposquamal side of the scale under hypocalcemic conditions but these data were not significantly different from the fluxes observed in isocalcemic conditions. When scales were subjected to a hypercalcemic environment (i.e., 3 mM Ca^{2+}), small influxes of Ca^{2+} were observed in the dorsal, ventral, and anterior regions on the episquamal side, but these were not significantly different from the fluxes measured under isocalcemic conditions. However, these Ca^{2+} influxes were significantly different in the dorsal ($P < 0.001$), ventral ($P < 0.01$), and anterior ($P < 0.05$) regions on the episquamal side, when compared with the effluxes observed under the hypocalcemic conditions. In addition, although small influxes were also (in general) observed on the hyposquamal side, the values were again not significantly different from those measured under isocalcemic conditions. Due to the overall similarities in the response of all three locations of the scale, Ca^{2+} fluxes were only measured on the episquamal and hyposquamal sides of the dorsal region in subsequent SIET-based experiments.

Determining the time-frame for the ex vivo culture of fish scales

The SIET Ca^{2+}-specific experiments typically lasted between approximately 50 min and 1 h, during which time, the scales were maintained in a solution that attempted to mimic the pH, osmolarity, and ionic composition of zebrafish plasma. It was therefore important to characterize the effect of the culturing conditions on the health of the scales; thus the effect of incubation duration on cell viability was determined.

There were two variables in this experiment: (1) the [Ca^{2+}] of the measuring medium, which was set to 0.01, 1.5, or 3 mM, and (2) the duration of incubation in the measuring medium (i.e., 0.5, 1, 2, or 4 h). Following these different treatments for varying lengths of time, scales were incubated with SYTO 11 and SYTOX orange (prepared in measuring medium at different [Ca^{2+}]) to label the nuclei of all cells and the nuclei of dead cells, respectively, and then the scales were fixed. Some scales were labeled with SYTO® 11 and SYTOX® orange immediately without any incubation time (i.e., time = 0 h), and these were used as positive controls for cell viability such that all (or the majority of) the cells were viable. In addition, some scales were fixed prior to labeling, as a negative control for the cell viability test, such that all the cells were dead. The percentage of live cells, calculated from the total number of cells (i.e., those with green or yellow nuclei) minus the number of dead cells (i.e., those with yellow nuclei) on fish scales ($n = 4$), after each treatment was quantified (Fig. 4). In the negative controls, in which the scales were fixed prior to labeling, the percentage of 'viable' cells was approximately 13.8% (see black dashed lines in Fig. 4a–d). To the contrary, scales that were labeled as soon as they were removed from the fish exhibited between 89.7 and 97.2% viable cells (such that the lowest viability of 89.7% was observed in 0.01 mM Ca^{2+}, and the highest viability of 97.2% viability was observed in 3 mM Ca^{2+}). There was also a high level of cell viability (i.e.

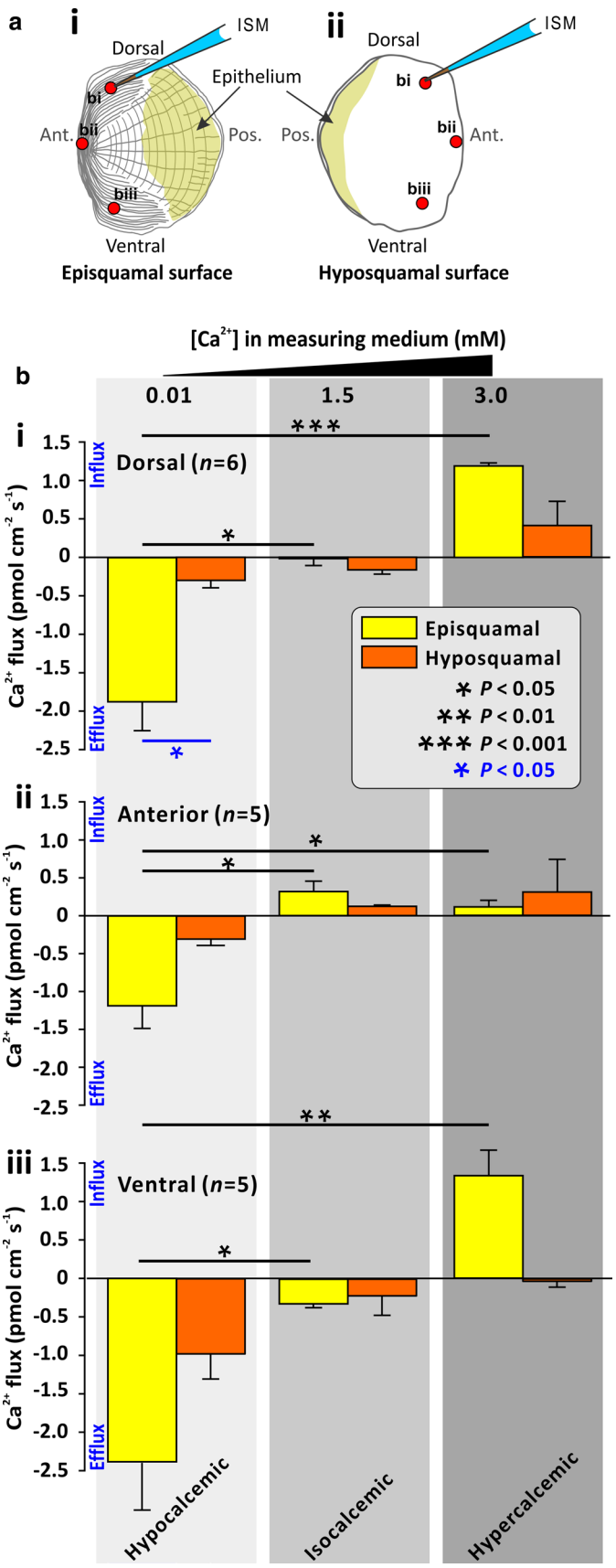

Fig. 3 Ca^{2+} flux measurements from the intact scales of approximately 1-year old male zebrafish. **a** Schematic illustrations of the episquamal (**ai**) and hyposquamal (**aii**) surfaces of a scale to show the regions scanned with the SIET system (see red circles). *Ant.* Anterior, *Pos.* posterior. **b** Bar graphs to show the mean ± standard error of the mean (SEM) values of Ca^{2+} flux measured 5 µm from the episquamal and hyposquamal surfaces of the scales in measuring medium containing 0.01, 1.5, or 3 mM Ca^{2+} (i.e., hypocalcemic, isocalcemic and hypercalcemic conditions respectively), in the dorsal (**bi**), anterior (**bii**), and ventral (**biii**) regions of the scale. The black asterisks indicate data that are significantly different when comparing Ca^{2+} flux values measured in the same region of the scales incubated in different extracellular Ca^{2+} concentrations ($[Ca^{2+}]_{ext.}$). The blue asterisk indicates data that are significantly different when comparing the Ca^{2+} flux values on the episquamal and hyposquamal sides when incubated in the same $[Ca^{2+}]_{ext.}$. For all significance data: $*P<0.05$, $**P<0.01$, and $***P<0.001$. The *P* values were determined by the Tukey–Kramer test after initial two-way analysis of variance (ANOVA) screening. No measurements were made in the posterior region of scales due to the presence of an obscuring layer of epithelial cells (color figure online)

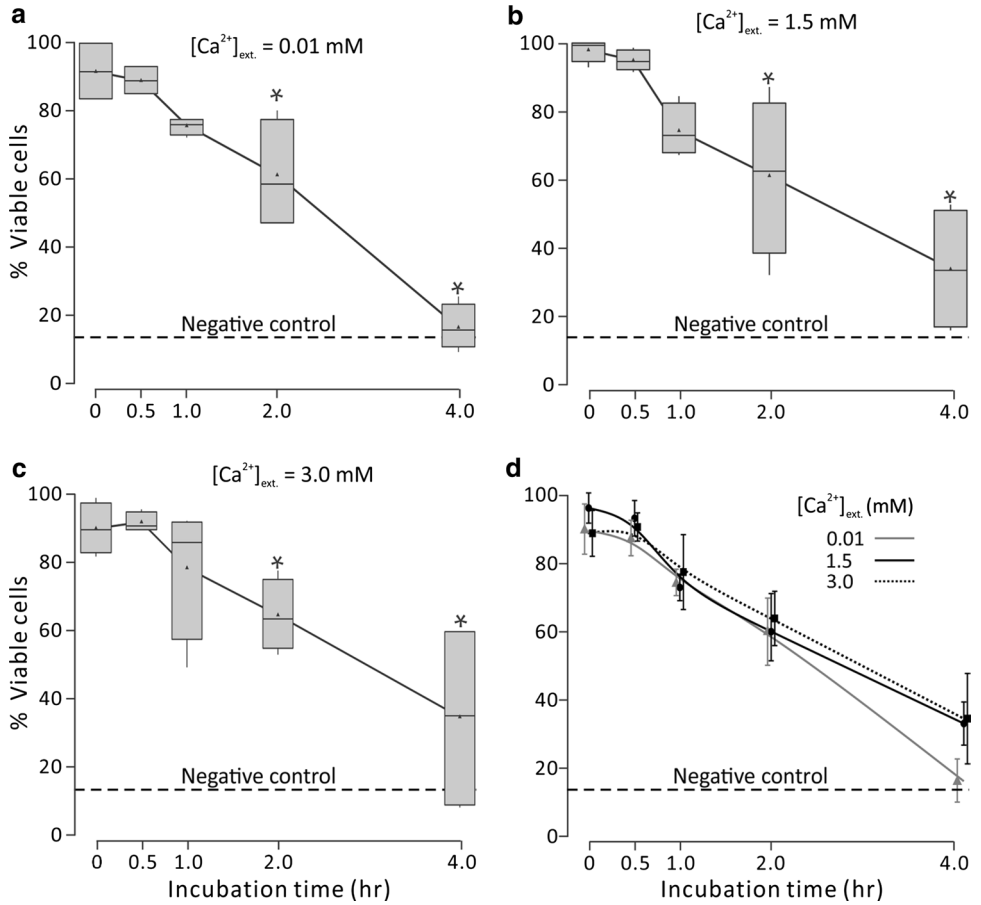

Fig. 4 Scale cell viability assay quantification. The number of nuclei were quantified in scales labeled with the SYTO® 11 and SYTOX® orange nucleic acid stains, using the DotCount image analysis software. **a**–**c** Box plots showing the percentage of viable cells in fish scales that were incubated in measuring medium containing 0.01 mM (**a**), 1.5 mM (**b**), or 3 mM (**c**) Ca^{2+}. The number of viable cells was determined by subtracting the number of dead cells (in which the nuclei were labeled with SYTOX® orange) from the total number of cells (in which the nuclei were labeled with SYTO® 11). In each graph, the Negative control is the percentage of viable cells quantified in the negative control group, in which the scales were fixed (cells were killed) prior to labeling of nuclei. The asterisks mark the time points in each treatment group that are significantly different from the positive control (0 h incubation) values (Tukey–Kramer test after two-way ANOVA screening, $P < 0.05$). **d** Graph comparing the percentage of viable cells in scales when incubated in measuring media with $[Ca^{2+}]_{ext.}$ at 0.01, 1.5, or 3 mM. No significant differences in the cell viability between the three $[Ca^{2+}]_{ext.}$ treatments at any time point were observed determined by two-way ANOVA

approx. 88.3–94.2%) when scales were bathed for just 0.5 h in measuring media at all three $[Ca^{2+}]$. In addition, after a 1-h incubation, the percentage cell viability was approximately 74.86, 73.56, and 77.99% for scales bathed in 0.01, 1.5, or 3.0 mM Ca^{2+}, respectively. There was no significant difference in the viability between the positive control (at 0 h of incubation) and the 0.5- and 1-h incubation time-points in all three treatments of measuring media $[Ca^{2+}]$ using the Tukey–Kramer test. When scales were incubated for 2 h in 0.01, 1.5, or 3.0 mM Ca^{2+}, then the cell viability decreased to approximately 60.58, 60.40, and 63.95%, respectively, and the cell viability decreased further after 4 h of incubation at all $[Ca^{2+}]_{ext.}$, when compared with the positive controls (i.e., with an incubation time of 0 h; $P < 0.05$). However, as shown in Fig. 4d, there was no significant difference in the overall cell viability between different $[Ca^{2+}]_{ext.}$. These data therefore indicate that the SIET measurements made with fish scales bathed in 0.01, 1.5, and 3.0 mM Ca^{2+}, which were conducted for < 1 h, involved cells that were largely viable.

Determining if the scale Ca^{2+} fluxes are biotic or abiotic in nature

In order to confirm that the SIET-based results obtained were due to biotic phenomena rather than abiotic processes, cells on the surface of exfoliated scales were killed by two different methods: (1) via dehydration followed by rehydration and (2) by treatment with 10 mM KCN.

Figure 5a shows the mean ± SEM Ca^{2+} flux values measured from dried/rehydrated scales placed in measuring

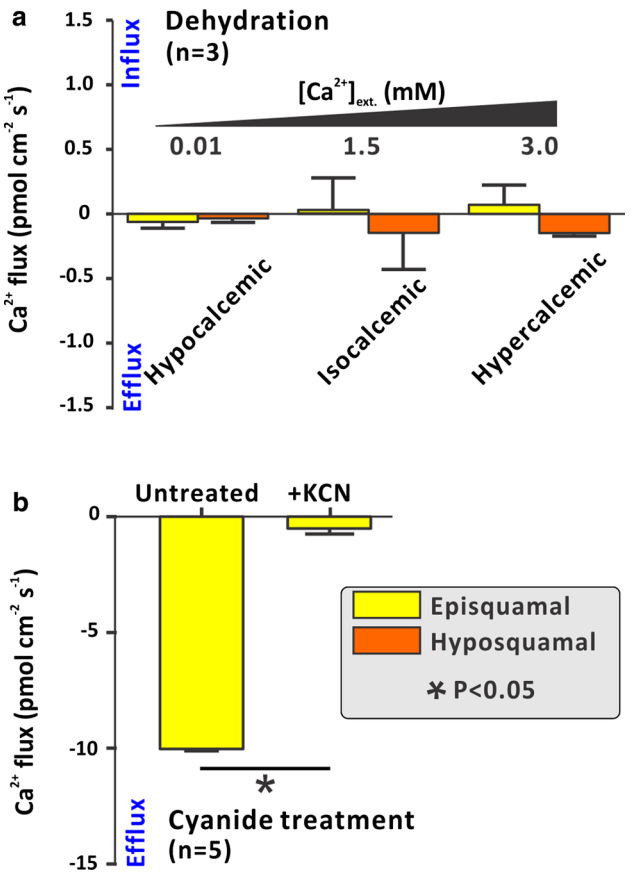

Fig. 5 The effect of dehydration or cyanide treatment on the Ca^{2+} fluxes generated by scales. **a** Bar graph showing the mean ± SEM Ca^{2+} fluxes generated after scales were killed by drying ($n = 3$). The Ca^{2+} fluxes measured at the episquamal surface were not significantly different from those generated at the hyposquamal surface, and those generated in the various $[Ca^{2+}]_{ext.}$ solutions were not significantly different from each other, as determined by two-way ANOVA. **b** Bar graph showing the effect of KCN on the Ca^{2+} fluxes generated by scales in $[Ca^{2+}]_{ext.}$ at 0.01 mM. The data show the mean ± SEM Ca^{2+} flux generated after scales were killed by treatment with 10 mM KCN ($n = 5$) compared with the untreated control. The asterisk indicates that the Ca^{2+} flux measured in dead scales (treated with KCN) was significantly different from that in the live (untreated control) scales, determined with the Student's *t* test ($P < 0.05$)

medium containing 0.01, 1.5, or 3 mM Ca^{2+}. The episquamal side of the scales exhibited a very small Ca^{2+} efflux (of − 0.06 ± 0.04 pmol/cm^2/s) when incubated in 0.01 mM Ca^{2+} and a small Ca^{2+} influx (of 0.07 ± 0.15 pmol/cm^2/s) when incubated in 3.0 mM Ca^{2+}. In addition, the hyposquamal side of rehydrated scales exhibited a small efflux of Ca^{2+} regardless of the $[Ca^{2+}]_{ext}$. However, none of the measurements made on the dried then rehydrated scales were significantly different from each other when compared using two-way ANOVA.

Figure 5b shows the effect of KCN treatment on the Ca^{2+} fluxes when compared with the untreated controls ($n = 5$ for each) when incubated in 0.01 mM Ca^{2+}. The data indicate that the Ca^{2+} flux generated in scales treated with KCN (− 0.52 ± 0.23 pmol/cm^2/s) was significantly different (at $P < 0.05$) from that in the untreated control group (− 10 ± 0.16 pmol/cm^2/s), when determined by the Student's *t* test.

Localization of Ca^{2+} deposits in scales

In an attempt to explain the pattern of real-time Ca^{2+} fluxes observed into and out of scales bathed in isocalcemic, hypercalcemic, or hypocalcemic solutions in the different regions of the scale (i.e., dorsal, ventral, and anterior) on the episquamal and hyposquamal surfaces, live or fixed scales were stained with the Ca^{2+}-binding dye, alizarin red S (Fig. 6). Figure 6a–c shows bright-field and alizarin red S fluorescence images of a representative scale. In these low-magnification views, more alizarin red S fluorescence is observed in the anterior and posterior regions of the scale. However, a superficial epithelium (Epi in Fig. 6) is present in the posterior region, which makes SIET measurements difficult in this region of the scale. For this reason, the posterior part of the scale was not included in our SIET experiments. In the higher magnification views (Fig. 6bi, bii) alizarin red S fluorescence can be observed in the dorsal and anterior regions of the scale, respectively. The yellow circles in Fig. 6b, bi and bii indicate the approximate regions where the SIET measurements were made. Thus, from the level of fluorescence, there appears to be more Ca^{2+} deposits in the anterior region of the scale than in the dorsal and ventral regions. When viewing sagittal sections of scales either stained with alizarin red S or when using transmission electron microscopy (Fig. 6di, dii, e), more Ca^{2+} deposits are localized at the episquamal side of the scale than at the hyposquamal side.

Discussion

In mammals, it is known that the bones of the axial skeleton play a crucial role both in the long-term remodeling of calcified structures in response to calciotropic challenges, as well as in the short-term minute-to-minute error correction of Ca^{2+} concentration in the ECF (ECF-$[Ca^{2+}]$) (Bronner 1992; Mundy and Guise 1999). In contrast, in fish it has been reported that for the long-term remodeling of calcified structures, Ca^{2+} is preferentially withdrawn from the scales (rather than the bones) in periods of high Ca^{2+} demand (Mugiya and Watabe 1977; Takagi et al. 1989; Persson et al. 1998, 1999; Kacem et al. 2013; Metz et al. 2014). Therefore, in fish, the scales appear to substitute for bone with regards to long-term homeostatic Ca^{2+} regulation. However, the objective of our new study was to explore whether scales might also contribute to short-term, minute-to-minute Ca^{2+}

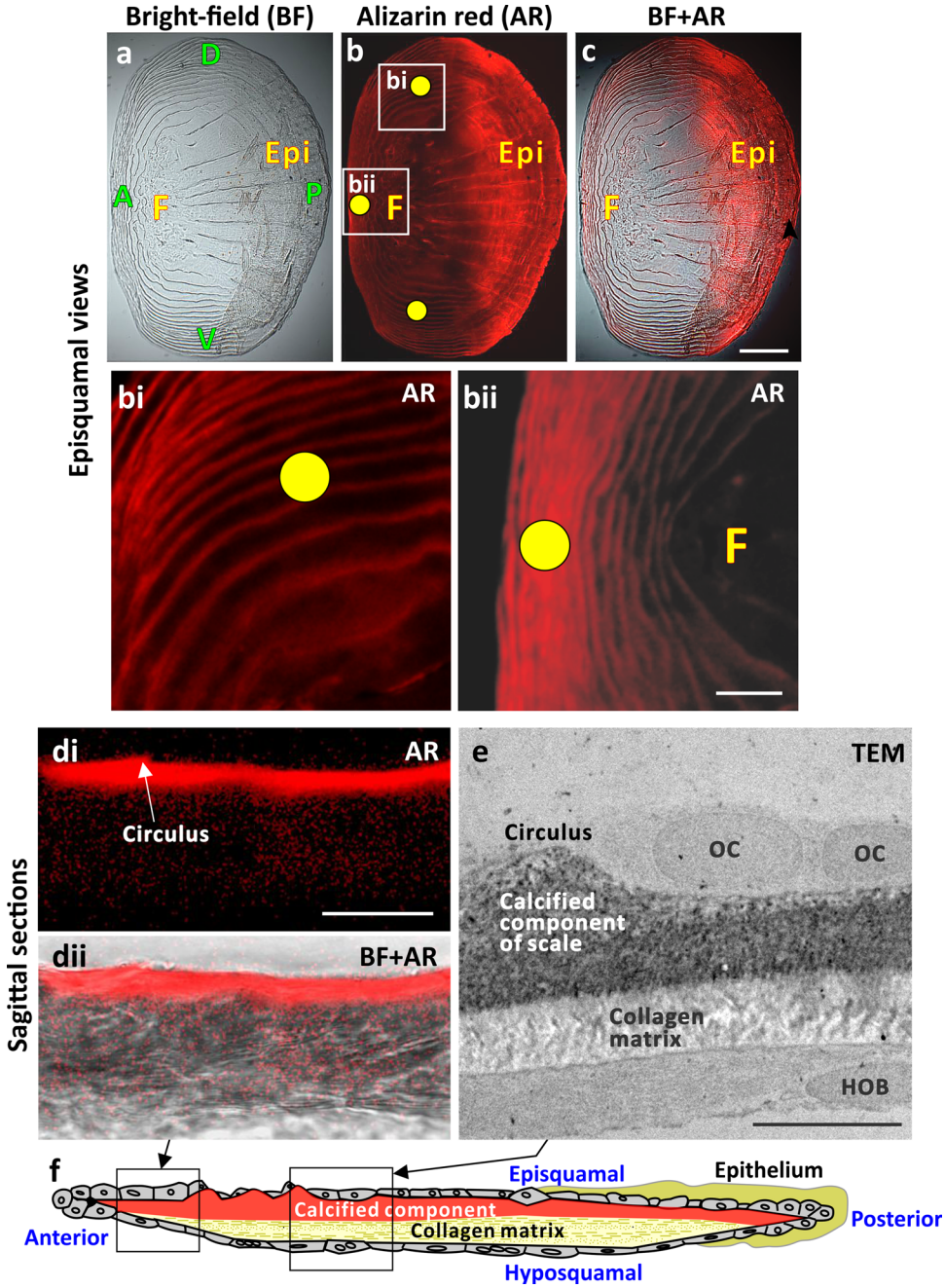

Fig. 6 Localization of Ca^{2+} in scales. **a**–**d** Representative images showing representative scales labeled with alizarin red S (*AR*). **a** Bright-field (*BR*), **b** AR fluorescence, **c** merged BR and AR fluorescence images. **bi**, **bii** Higher magnification images of the regions bounded by the white squares in **b**, which show elevated levels of Ca^{2+} localized in the dorsal lateral region (**bi**) and the anterior region (**bii**) of the scale. *A* Anterior, *P* posterior, *D* dorsal, *V* ventral, *F* focus, *Epi* epithelial layer; yellow circles indicate the regions scanned by the SIET system. **di**, **dii** Sagittal sections of scales labeled with AR, with **di** showing the localization of AR fluorescence alone and **dii** showing a merged BR and AR fluorescence image. **e** Sagittal transmission electron microscopy (*TEM*) section of a scale showing two osteocytes (*OC*) located near to a circulus, and one osteoblast located on the hyposquamal side of the scale (*HOB*). **f** Schematic illustration of a scale showing the approximate locations of the images shown in **di**, **dii**, **e**. Scale bars: 200 µm (**a**–**c**), 50 µm (**bi**, **bii**), 20 µm (**di**, **dii**), 5 µm (**e**) (color figure online)

exchange, and if they do so, is it via a similar mechanism to that reported from mammalian bone (Marenzana et al. 2005; Dedic et al. 2018; Hohman et al. 2018)? In particular, we focused on: (1) the possible role played by a putative readily-exchangeable Ca^{2+} storage pool (or pools) between the biotic/abiotic regions of the scales and the ECF and (2) the particular side of the scale involved in this short-term Ca^{2+} exchange. As is the case with mammals, fish do not rely exclusively on a single mechanism to achieve short-term regulation of the ECF-$[Ca^{2+}]$; for example, rapid Ca^{2+} exchange across the gills contributes to this process (Wendelaar Bonga and Flik 1993; Hwang et al. 2011). However, in order to meet a number of different challenges it might be advantageous for fish to be able to also rapidly exchange Ca^{2+} ions between their ECF and scales in a manner that does not involve long-term scale remodeling. For example, fish might experience rapid short-term calcemic challenges, such as those resulting from integument wounding (Viera et al. 2011), and/or sudden inflows of saline water into normally fresh water environments (Herbert et al. 2015). These may differ from longer-term physiological, environmental, behavioral, or reproductive-derived calcemic challenges

(or a combination of any of these) that accumulate over extended periods of time whereby longer-term homeostatic mechanisms, such as scale remodeling, resolve the calcemic imbalance. Examples of the latter scenarios might arise in diadromous fish returning from salt water to spawn in fresh water or vice versa (Kacem et al. 2013), or where there is a high seasonal Ca^{2+} demand in female fish resulting from vitellogenesis (Persson et al. 1998; Guerrerio et al. 2002) and/or oogenesis (Golpour et al. 2016). Thus, the possession of both long- and short-term restorative mechanisms, with the latter relying on a readily-exchangeable Ca^{2+} store, might offer distinct selective advantages (Lin and Hwang 2016).

We report that in the absence of any local or systemic regulators, exfoliated scales reacted in a predictable and rapid manner to external calcemic challenges that were designed to mimic changes in the ECF-[Ca^{2+}]. As in mammals, the design of a balanced scale bathing solution containing all of the ions required for the physiological functioning of biomineralization events is highly challenging (Tas 2014). We therefore maintained the exfoliated scales in a bathing medium that essentially approximated the composition and the overall ionic strength of the ECF. We made the assumption that in zebrafish, the ECF-[Ca^{2+}] is approximately 1.5 mM (Nakari and Erkomaa 2003), which is similar to that reported for other fresh water teleosts, such as the Rainbow Trout (*Salmo gairdneri*; Andreasan 1985). It is also similar to the ionized plasma [Ca^{2+}] of the euryhaline flounder, *Platichthys flesus*, which also sustains low salinity levels and spends part of its life cycle in freshwater (Lu et al. 2017). Thus, when the exfoliated scales of zebrafish were maintained in bathing medium, which we defined as being isocalcemic (where [Ca^{2+}] = 1.5 mM), a minimal flux of Ca^{2+} ions was elicited at all three measuring positions chosen, i.e., dorsal, ventral, and anterior, on either side of the scale (Fig. 3b), thus indicating an approximate equilibrium condition. However, when the scale was challenged by either a hypocalcemic (0.01 mM Ca^{2+}) or a hypercalcemic (3.0 mM Ca^{2+}) bathing medium, a predictable outward and inward flux of Ca^{2+} ions, respectively, was detected within approximately 3 min after the start of measurement on either side of the scale. The Ca^{2+} efflux was consistently greater on the episquamal side than on the hyposquamal side under hypocalcemic conditions. Moreover, the Ca^{2+} influx was also consistently higher on the episquamal side than the hyposquamal side under hypercalcemic conditions. The only exception was that a small Ca^{2+} efflux was detected at the ventral measuring position on the hyposquamal side under a hypercalcemic challenge (Fig. 3biii). Thus, overall, the cells on the episquamal side of the scale appeared to be more active in generating Ca^{2+} fluxes than those on the hyposquamal side, when challenged by different calcemic conditions. This might reflect the fact that this side of the scale presents a larger surface area due to the surface topology (Meunier 1984; Sire and Akimenko 2004), and its cell populations are to some extent protected in the troughs between the circuli ridges (De Vrieze et al. 2010; Pasqualetti et al. 2012b).

Dehydration and KCN treatment of the scales demonstrated that the Ca^{2+} fluxes measured under different calcemic challenges were biotic in nature (Fig. 5a, b). These results suggest that the fluxes were generated by active trans-membrane Ca^{2+} transport processes, such as plasma membrane Ca^{2+}-ATPases and/or via Na^{+}/Ca^{2+} exchangers, in the case of Ca^{2+} efflux, and as a result of the activation/opening of some form of membrane Ca^{2+} channel or the generation of some form of transcellular Ca^{2+} transport in the case of Ca^{2+} influx. However, the molecular identification of these specific Ca^{2+} transport elements in scales requires further investigation. It has been reported that there are stores of non-crystalline Ca^{2+} phosphate within the internal layer of tilapia (*Oreochromis niloticus*) scales (Okuda et al. 2011). We suggest that this might contribute to a readily-exchangeable short-term Ca^{2+} store that does not involve the long-term remodeling of crystalline hydroxyapatite deposits within scales. Furthermore, an alternative readily-exchangeable Ca^{2+} store might also be found in the intracellular organelles of the cells covering the surface of the scale, such as the ER, mitochondria, and acid vesicles (Berridge et al. 2003), as well as being bound to various cytoplasmic Ca^{2+} buffers, such as parvalbumins, calbindins, and calretinins (Gilabert 2012). Identifying the molecular components of the Ca^{2+} deposition and resorption pathways, as well as the specific Ca^{2+} stores involved, will be the next step in our continuing study.

Support for the use of zebrafish and their scales as viable complementary models for both basic and clinical mammalian bone research continues to accumulate despite two challenges: (1) the long evolutionary distance that separates zebrafish and mammals (Donoghue and Sansom 2002; Sire and Huysseune 2003; Hirasawa and Karatani 2015); (2) the difficulty in connecting teleost genes and gene function to human biology due to (amongst other things) two rounds of early vertebrate genome duplication (Dehal and Boore 2005). In addition to our new findings, a number of other key features support the benefits of using these models for studying many aspects of mammalian biology: (1) a shared mesodermal origin (Mongera and Nüsslein-Volhard 2013; Lee et al. 2013; Shimada et al. 2013); (2) developmental and genetic similarities (Nakamura et al. 2016); (3) shared basic components, including osteoclasts (de Vrieze et al. 2011; Sharif et al. 2014), osteoblasts (Kitamura et al. 2013), hydroxyapatite crystals (Mariotti et al. 2015), matrix proteins, collagen fibers, and Ca^{2+} storage proteins (de Vrieze et al. 2011; Metz et al. 2012; Pasqualetti et al. 2012a); (4) intimate three-dimensional spatial relationships of their components, e.g., between cells and the mineralized matrix (Weiner and Wagner 1998; Sire and Akimenko 2004); and

(5) response to common systemic Ca^{2+} regulators (Rubin and Jüppner 1999; Craig et al. 2008; Suzuki et al. 2011).

We suggest, therefore, that our new evidence supports the proposition that elasmoid scales of zebrafish might provide a valuable, cost-effective, genetically-tractable non-mammalian model to investigate the health-related consequences of errors in ECF-[Ca^{2+}] homeostasis that are not adequately adjusted by short-term correction mechanisms, similar to those that have been reported to be present in mammalian bones (Marenzana et al. 2005; Dedic et al. 2018). Furthermore, the effect of hormones, drugs, and novel active compounds on short-term correction mechanisms can initially be tested in real time in the relatively simple and inexpensive zebrafish scale model, before they are verified in mammalian bone models. Together, our data add to the accumulating body of evidence suggesting that fish scales might prove to be a suitable, complementary model to study mammalian bone development, disease, injury, repair, and regeneration (Yoshikubo et al. 2005; Metz et al. 2012, 2014; Pasqualetti et al. 2012b; Laizé et al. 2014; Mariotti et al. 2015; Suzuki et al. 2016a, b). We also suggest that our new study has the potential to produce therapeutic insights and thus help improve life quality and expectancy in individuals for whom short-term dysfunction of Ca^{2+} homeostasis might lead to an increase in renal impairment (Moysés-Neto et al. 2006), cardiovascular damage (Wang et al. 2014), and bone fragility fracture risk. Regarding the latter, it has been shown that the extracellular Ca^{2+} concentration modulates the cell-dependent mineralization process of the bone matrix (Majore et al. 2007; Welldon et al. 2013), which is an established determinant of the mechanical behavior of bone (reviewed by Unal et al. 2018).

We suggest that in the SIET experiments, the differences in the fluxes observed both into and out of scales might be explained by the relative position of the surface cells with respect to the Ca^{2+} deposits within the scale, which are located mainly in the episquamal side, and more in the anterior regions of this side of the scale (Fig. 6). This might explain why the cells on the episquamal side of the scale always generated larger Ca^{2+} fluxes than those on the hyposquamal side. Even though we demonstrated that the Ca^{2+} fluxes recorded were biotic in nature (Fig. 5) and thus not generated by abiotic Ca^{2+} deposits within the scale, it has been reported that extracellular Ca^{2+} can regulate the function of bone-associated cells (reviewed by Hofer 2005; Breitwieser 2008). For example, it has been reported that high concentrations of extracellular Ca^{2+} can promote the migration, proliferation, and maturation of osteoblasts in bone (Sugimoto et al. 1993), and fluctuations in extracellular Ca^{2+} might integrate cell signaling responses in multicellular networks via the activation of a Ca^{2+}-sensing receptor (De Luisa and Hofer 2003). Thus, we suggest that there might be a gradient of extracellular Ca^{2+} in the intercellular space within zebrafish scales, with the highest level being located just under the episquamal surface, and that this gradient might in some way influence the activity of the surface cells on the episquamal and hyposquamal surfaces. Our investigations to determine if this is indeed the case are ongoing.

Acknowledgements This project was supported by the Hong Kong Research Grants Council General Research Fund awards: 16101714 and 16100115. We also acknowledge funding from the Hong Kong Innovation and Technology Commission (ITCPD/17-9). This work was made possible by equipment and support generously provided by Mr. Chris Shipley of Applicable Electronics, LLC., New Haven, CT, USA, and software kindly donated by Mr. Eric Karplus of Science Wares Inc., Falmouth, MA, USA. Initial experiments were carried out by JTH at the MBL (Woods Hole) during the Croucher Foundation-funded JUSTL Program.

Author contributions JTH was involved in developing the methodology, conducting the research, and preparing the manuscript. SEW helped to supervise the project and was involved with conducting the research, verifying the results, and preparing the manuscript. CP was involved in conducting some of the research and preparing the manuscript. AML was involved in conducting some of the research. AMS helped design the methodology, provided the instrumentation, and helped with student training. AR helped to formulate the research goals and was involved in preparing the manuscript. JGK helped to formulate the research goals and provided advice regarding the methodology and data analysis. ALM formulated the overarching research goals, supervised the project, provided the resources for conducting the project, and prepared the manuscript. All the authors helped review the manuscript.

References

Ablain J, Zon LI (2013) Of fish and men: using zebrafish to fight human diseases. Trends Cell Biol 23:584–586

Andreasan P (1985) Free and total calcium concentrations in the blood of rainbow trout, *Salmo gairdneri*, during 'stress' conditions. J Exp Biol 118:111–120

Bakkers J (2011) Zebrafish as a model to study cardiac development and human cardiac disease. Cardiovasc Res 91:279–288

Berridge MJ, Bootman MD, Roderick HL (2003) Calcium signalling: dynamics, homeostasis and remodelling. Nat Rev Mol Cell Biol 4:517–529

Blaine J, Chonchol M, Levi M (2014) Renal control of calcium, phosphate, and magnesium homeostasis. Clin J Am Soc Nephrol 10:1257–1272

Breitwieser GE (2008) Extracellular calcium as an integrator of tissue function. Int J Biochem Cell Biol 40:1467–1480

Bronner F (1992) Bone and calcium homeostasis. Neurotoxicology 13:775–782

Burns CG, MacRae CA (2006) Purification of hearts from zebrafish embryos. Biotechniques 40:274 (276, 278)

Catté M, Dussap C-G, Gros J-B (1995) A physical chemical UNIFAC model for aqueous solutions of sugars. Fluid Phase Equilib 105:1–25

Craig TA, Sommer S, Sussman CR, Grande JP, Kumar R (2008) Expression and regulation of the vitamin D receptor in the zebrafish, *Danio rerio*. J Bone Mineral Res 23:1486–1496

De Luisa A, Hofer AM (2003) Evidence that Ca^{2+} cycling by the plasma membrane Ca^{2+}-ATPase increases the 'excitability' of the extracellular Ca^{2+}-sensing receptor. J Cell Sci 116:1527–1538

De Vrieze E, Metz JR, Von den Hoff JW, Flik G (2010) ALP, TRAcP, and cathepsin K in elasmoid scales; a role in mineral metabolism? J Appl Ichthyol 26:210–213
De Vrieze E, Sharif F, Metz JR, Flik G, Richardson MK (2011) Matrix metalloproteinases in osteoclast of ontogenetic and regenerating zebrafish scales. Bone 48:704–722
Dedic C, Hung JT, Shipley AM, Maeda A, Gardella T, Miller AL, Divieti Pajevic P, Kunkel J, Rubinacci A (2018) Calcium fluxes at the bone-plasma interface: acute effects of parathyroid hormone (PTH) and targeted deletion of PTH/PTH-related peptide (PTHrP) receptor in the osteocyte. Bone 116:135–143
Dehal P, Boore JL (2005) Two rounds of whole genome duplication in the ancestral vertebrate. PLoS Biol 3(10):e314. https://doi.org/10.1371/journal.pbio.0030314
Donoghue PC, Sansom IJ (2002) Origin and early evolution of vertebrate skeletonization. Microsc Res Tech 59:352–372
Dooley K, Zon LI (2000) Zebrafish: a model system for the study of human disease. Curr Opin Gen Devel 10:252–256
Elliott DG (2000) Integumenatry system. In: Ostrander GK (ed) Handbook of experimental animals: the laboratory fish. Academic Press, Cambridge, pp 271–306
Flik G, Verbost PM (1993) Calcium transport in fish gills and intestine. J Exp Biol 184:17–29
Flik G, Fenwick JC, Kolar Z, Mayer-Gostan N, Wendelaar Bonga SE (1986) Effects of low ambient calcium levels on wholebody Ca^{2+} flux rates and internal calcium pools in the freshwater teleost, *Oreochromis mossambicus*. J Exp Biol 120:249–264
Flik G, Verbost PM, Wendelaar Bonga SE (1995) Calcium transport processes in fishes. Fish Physiol 14:317–342
Gilabert JA (2012) Cytoplasmic calcium buffering. In: Islam M (ed) Calcium signaling. Advances in experimental medicine and biology. Springer, Dordrecht, pp 483–498
Goldberg RN (1981) Evaluated activity and osmotic coefficients for aqueous solutions: thirty-six uni-bivalent electrolytes. J Phys Chem Ref Data 10:671–764
Goldberg RN, Nuttall RL (1978) Evaluated activity and osmotic coefficients for aqueous solutions: the alkaline earth metal halides. J Phys Chem Ref Data 7:263–310
Goldsmith JR, Jobin C (2012) Think small: zebrafish as a model system of human pathology. J Biomed Biotech 2012:817341. https://doi.org/10.1155/2012/817341
Golpour A, Pšenička M, Niksirat H (2016) Subcellular localizations of calcium deposits during zebrafish (*Danio rerio*) oogenesis. Micron 80:6–13
Greenwood MP, Flik G, Wagner GF, Balment RJ (2009) The corpuscles of Stannius, calcium-sensing receptor, and stanniocalcin: responses to calcimimetics and physiological challenges. Endocrinology 150:3002–3010
Guerrerio PM, Fuentes J, Canário AVM, Power DM (2002) Calcium balance in sea bream (*Sparus aurata*): the effect of oestradiol-17β. J Endocrinol 173:377–385
Guh YJ, Lin CH, Hwang PP (2015) Osmoregulation in zebrafish: ion transport mechanisms and functional regulation. Exp Clin Sci J 14:627–659
Hamer WJ, Wu Y-C (1972) Osmotic coefficients and mean activity coefficients of uni-univalent electrolytes in water at 25 °C. J Phys Chem Ref Data 1:1047–1100
Herbert ER, Boon P, Burgin AJ, Neubauer SC, Franklin RB, Ardón M, Hopfensperger KN, Lamers LPM, Gell P (2015) A global perspective on wetland salinization: ecological consequences of a growing threat to freshwater wetlands. Ecosphere 6(10):1–43. https://doi.org/10.1890/ES14-00534.1
Hirasawa T, Karatani S (2015) Evolution of the vertebrate skeleton: morphology, embryology, and development. Zool Lett 1:2. https://doi.org/10.1186/s40851-014-0007-7
Hofer AM (2005) Another dimension to calcium signaling: a look at extracellular calcium. J Cell Sci 118:855–862
Hohman EE, Hodges JK, Wastney ME, Lacheik PJ, Han CY, Dwyer D, Peacock M, Kostenuik PJ, Weaver CM (2018) Serum calcium concentration is maintained when bone resorption is suppressed by osteoprotegerin in young growing male rats. Bone 116:162–170
Hwang PP, Chou MY (2013) Zebrafish as an animal model to study ion homeostasis. Pflugers Arch Eur J Physiol 465:1233–1247
Hwang PP, Lee TH, Lin LY (2011) Ion regulation in fish gills: recent progress in the cellular and molecular mechanisms. Am J Physiol Regul Integr Comp Physiol 301:R28–R47
Ingham PW (2009) The power of zebrafish for disease analysis. Human Mol Genet 18:R107–R112
Iwasaki M, Kuroda J, Kawakami K, Wada H (2018) Epidermal regulation of bone morphogenesis through the development and regeneration of osteoblasts in the zebrafish scale. Dev Biol 437:105–119
Kacem A, Baglinière JL, Meunier FJ (2013) Resorption of scales in Atlantic salmon (*Salmo salar*) during its anadromous migration: a quantitative study. Cybium: Revue Internationale d'Ichtyologie 37:199–206
Kalueff AV, Stewart AM, Gerlai R (2014) Zebrafish as an emerging model for studying complex brain disorders. Trends Pharmacol Sci 35:63–75
Kinkel MD, Eames SC, Philipson LH, Prince VE (2010) Intraperitoneal injection into adult zebrafish. J Vis Exp. https://doi.org/10.3791/2126
Kitamura K, Takahira K, Inari M, Satoh Y, Hayakawa K, Tabuchi Y, Ogai K, Nishiuchi T, Kondo T, Mikuni-Takagaki Y, Chan W, Hattori A, Suzuki N (2013) Zebrafish scales respond differently to in vitro dynamic and static acceleration: analysis of interaction between osteoblasts and osteoclasts. Comp Biochem Physiol Part A Mol Integr Physiol 166:74–80
Kühtreiber WM, Jaffe LF (1990) Detection of extracellular calcium gradients with a calcium-specific vibrating electrode. J Cell Biol 110:1565–1573
Kunkel JG, Cordeiro S, Xu Y, Shipley AM, Feijó JA (2006) Use of non-invasive ion-selective microelectrode for the study of plant development. In: Volkov AG (ed) Plant electrophysiology. Springer, Berlin, pp 109–137
Kwong RW, Kumai Y, Perry SF (2016) Neuroendocrine control of ionic balance in zebrafish. Gen Comp Endocrinol 234:40–46
Laizé V, Gavaia PJ, Cancela ML (2014) Fish: a suitable system to model human bone disorders and discover drugs with osteogenic or osteotoxic activities. Drug Discov Today Dis Mod 13:29–37
Lee RTH, Thiery JP, Carney TJ (2013) Dermal fin rays and scales derive from mesoderm, not neural crest. Curr Biol 23:R336–R337
Lin CH, Hwang PP (2016) The control of calcium metabolism in zebrafish (*Danio rerio*). Int J Mol Sci. https://doi.org/10.3390/ijms17111738
Lin C-Y, Chiang C-Y, Tsai HJ (2016) Zebrafish and medaka: New model organisms for modern biomedical research. J Biomed Sci 23:19. https://doi.org/10.1186/s12929-016-0236-5
Lu W, Jin Y, Xu J, Greenwood MP, Balment RJ (2017) Molecular characterisation and expression of parathyroid hormone-related protein in the caudal neurosecretory system of the euryhaline flounder, *Platichthys flesus*. Gen Comp Endocrinol 249:24–31
Majore I, Jager V, Rohde M (2007) Influence of extracellular calcium concentration on the bone matrix synthesis and mineralization in cultures of human primary osteoprogenitor cells. J Stem Cell Regen Med 2:125–126
Marenzana M, Shipley AM, Squitiero P, Kunkel JG, Rubinacci A (2005) Bone as an ion exchange organ: evidence for

instantaneous cell-dependent calcium efflux from bone not due to resorption. Bone 37:545–554
Mariotti M, Carnovali M, Banfi G (2015) *Danio rerio*: the Janus of the bone from embryo to scale. Clin Cases Min Bone Metab 12:188–194
Metz JR, De Vrieze E, Lock EJ, Schulten IE, Flik G (2012) Elasmoid scales of fishes as a model in biomedical bone research. J Appl Ichthyol 28:382–387
Metz JR, Leeuwis RHJ, Zethof J, Flik G (2014) Zebrafish (*Danio rerio*) in calcium-poor water mobilize calcium and phosphorus from scales. J Appl Ichthyol 30:671–677
Meunier FJ (1984) Spatial organization and mineralization of the basal plate of the elasmoid scales in osteichthyans. Am Zool 24:953–964
Mongera A, Nüsslein-Volhard C (2013) Scales of fish arise from mesoderm. Curr Biol 23:338–339
Moysés-Neto M, Guimarães FM, Ayoub FH, Vieira-Neto OM, Costa JAC, Dantas M (2006) Acute renal failure and hypercalcemia. Ren Fail 28:153–159
Mugiya Y, Watabe N (1977) Studies on fish scale formation and resorption. II. Effect of estradiol on calcium homeostasis and skeletal tissue resorption in the goldfish, *Carassius auratus*, and the killifish, *Fundulus heteroclitus*. Comp Biochem Physiol A Physiol 57:197–202
Mundy GR, Guise TA (1999) Hormonal control of calcium homeostasis. Clin Chem 45:1347–1352
Nakamura T, Gehrke AR, Lemberg J, Szymaszek J, Shubin NH (2016) Digits and fin rays share common developmental histories. Nature 537:225–228
Nakari T, Erkomaa K (2003) Effects of phytosterols on zebrafish reproduction in multigeneration test. Environ Pollut 123:267–273
Ogawa N, Ura K, Takagi Y (2010) Scale calcification in the goldfish in vitro: histological and quantitative analysis. Fish Sci 76:189–198
Okuda M, Ogawa N, Takeguchi M, Hashimoto A, Tagaya M, Chen S, Hanagata N, Ikoma T (2011) Minerals and aligned collagen fibrils in tilapia fish scales: structural analysis using dark-field and energy-filtered transmission electron microscopy and electron tomography. Microsc Microanal 17:788–798
Pan C (1977) Activity and osmotic coefficients in dilute aqueous solutions of bi-univalent electrolytes at 25 °C. J Chem Eng Data 22:234–237
Pasqualetti S, Banfi G, Mariotti M (2012a) Osteoblast and osteoclast behavior in zebrafish cultured scales. Cell Tissue Res 350:69–75
Pasqualetti S, Banfi G, Mariotti M (2012b) The zebrafish scale as a model to study the bone mineralization process. J Mol Histol 43:589–595
Persson P, Sundell K, Björnsson BT, Lundqvist H (1998) Calcium metabolism and osmoregulation during sexual maturation of river running Atlantic salmon. J Fish Biol 52:334–349
Persson P, Björnsson BT, Takagi Y (1999) Characterisation of morphology and physiological actions of scale osteoclasts in the rainbow trout. J Fish Biol 54:669–684
Persson P, Shrimpton JM, McCormick SD, Björnsson BT (2000) The presence of high-affinity, low capacity estradiol-17β binding in rainbow trout scale indicates a possible endocrine route for the regulation of scale resorption. Gen Comp Endocrinol 120:35–43
Pitzer KS, Peiper JC (1979) Activity coefficient of aqueous $NaHCO_3$. J Phys Chem 84:2396–2398
Rard JA, Miller DG (1981) Isopiestic determination of the osmotic coefficients of aqueous Na_2SO_4, $MgSO_4$, and Na_2SO_4–$MgSO_4$ at 25 °C. J Chem Eng Data 26:33–38
Reid B, Zhao M (2011) Ion-selective self-referencing probes for measuring specific ion flux. Commun Integr Biol 4:524–527
Reuter M (2012) DotCount software. Cambridge https://reuter.mit.edu/software/dotcount/
Rotllant J, Redrullo B, Guerreiro PM, Fernandes H, Canario AMV, Power DM (2005) Calcium mobilization from fish scales in mediated by parathyroid hormone related protein via the parathyroid hormone receptor type 1 receptor. Regul Peptides 132:33–40
Rubin DA, Jüppner H (1999) Zebrafish express the common parathyroid hormone/parathyroid hormone-related peptide receptor (PTH1R) and a novel receptor (PTH3R) that is preferentially activated by mammalian and fugufish parathyroid hormone-related peptide. J Biol Chem 274:28185–28190
Schneider CA, Rasband WS, Eliceiri KW (2012) NIH Image to ImageJ: 25 years of image analysis. Nat Methods 9:671–675
Schönbörner AA, Boivin G, Baud CV (1979) The mineralization process in teleost fish scales. Cell Tissue Res 202:203–212
Sharif F, de Bakker MAG, Richardson MK (2014) Osteoclast-like cells in early zebrafish embryos. Cell J 16:211–224
Shi WC, Fang ZB, Li L, Luo LF (2015) Using zebrafish as the model organism to understand organ regeneration. Sci China Life Sci 58:343–351
Shimada A, Kawanishi T, Kaneko T, Yoshihara H, Yano T, Inohaya K, Kinoshita M, Kamei Y, Yamura K, Takeda H (2013) Trunk exoskeleton in teleosts is mesodermal in origin. Nat Commun. https://doi.org/10.1038/ncomms2643
Shipley AM (2009) Scanning microelectrode techniques (SIET/SPET) system manual. Applicable Electronics Inc, Forestdale
Sionkowska A, Kozlowska J (2013) Fish scales as a biocomposite of collagen and calcium salts. Key Eng Mater 587:185–190
Sire JY, Akimenko MA (2004) Scale development in fish: A review, with description of sonic hedgehog (shh) expression in the zebrafish (*Danio rerio*). Int J Dev Biol 48:233–247
Sire JY, Huysseune A (2003) Formation of dermal skeleton and dental tissues in fish: a comparative and evolutionary approach. Biol Rev Camb Philos Soc 78:219–249
Sire JY, Allizard F, Babiar O, Bourguignon J, Quilhac S (1997) Scale development in zebrafish (*Danio rerio*). J Anat 190:545–561
Sire JY, Girondot M, Babiar O (2000) Marking zebrafish, *Danio rerio* (cyprinidae), using scale regeneration. J Exp Zool 286:297–304
Smith PJ, Hammar K, Porterfield DM, Sanger RH, Trimarchi JR (1999) Self-referencing, non-invasive, ion selective electrode for single cell detection of trans-plasma membrane calcium flux. Micro Res Tech 46:398–417
Sugimoto T, Kanatani M, Kano J, Kaji H, Tsukamoto T, Yamaguchi T, Fukase M, Chihara K (1993) Effects of high calcium concentration on the functions and interactions of osteoblastic cells and monocytes and on the formation of osteoclast-like cells. J Bone Miner Res 8:1445–1452
Suzuki N, Danks JA, Maruyama Y, Ikegame M, Sasayama Y, Hattori A, Nakamura M, Tabata MJ, Yamamoto T, Furuya R, Saijoh K, Mishima H, Srivastav AK, Furusawa Y, Kondo T, Tabuchi Y, Takasaki I, Chowdhury VS, Hayakawa K, Martin TJ (2011) Parathyroid hormone 1(1–34) acts on the scales and involves calcium metabolism in goldfish. Bone 48:1186–1193
Suzuki N, Hanmoto T, Yano S, Furusawa Y, Ikegame M, Tabuchi Y, Kondo T, Kitamura K, Endo M, Yamamoto T, Sekiguchi T, Urata M, Mikuni-Takagaki Y, Hattori A (2016a) Low-intensity pulsated ultrasound induces apoptosis is osteoclasts: Fish scales are suitable model for the analysis of bone metabolism. Comp Biochem Physiol A Mol Integr Physiol 195:26–31
Suzuki N, Kitamura K, Hattori A (2016b) Fish scale is a suitable model for analyzing determinants of skeletal fragility in type-2 diabetes. Endocrine 54:575–577
Takagi Y, Hirano T, Yamada J (1989) Scale regeneration of tilapia (*Oreochromis niloticus*) under various ambient and dietary calcium concentrations. Comp Biochem Physiol A Physiol 92:605–608

Tas CA (2014) The use of physiological solutions or media in calcium phosphate synthesis and processing. Acta Biomater 10:1771–1792

Unal M, Creecy A, Nyman JS (2018) The role of matrix composition in the mechanical behavior of bone. Curr Osterporos Rep 16:205–215

Viera FA, Gregorio SF, Ferraresso S, Thorne MAS, Costa R, Milan M, Bargelloni L, Clark MS, Canario AVM, Power DM (2011) Skin healing and scale regeneration in fed and unfed sea bream, *Sparus auratus*. BMC Genomics 12:490. https://doi.org/10.1186/1471-2164-12-490

Wang X, Chen H, Ouyang Y, Liu J, Zhao G, Bao W, Yan M (2014) Dietary calcium intake and mortality risk from cardiovascular disease and all causes: a meta-analysis of prospective cohort studies. BMC Med 12:158. https://doi.org/10.1186/s12916-014-0158-6

Waterman RE (1970) Fine structure of scale development in the teleost, *Brachydanio rerio*. Anat Rec 168:361–379

Weiner S, Wagner HD (1998) The material bone: structure–mechanical function relations. Ann Rev Mat Sci 28:271–298

Welldon KJ, Findlay DM, Evdokiou A, Ormsby RT, Atkins GJ (2013) Calcium induces pro-anabolic effects on human primary osteoblasts associated with acquisition of mature osteocyte markers. Mol Cell Endocrinol 376:85–92

Wendelaar Bonga SE, Flik G (1993) Calcium regulation in fish. In: Lahlou B, Vitiello P (eds) Aquaculture: fundamental and applied research. American Geophysical Union, New York, pp 47–59

Westerfield M (2000) The Zebrafish book: a guide for the laboratory use of zebrafish (*Danio rerio*). University of Oregon Press, Corvallis

Yoshikubo H, Suzuki N, Takemura K, Hoso M, Yashima S, Iwamuro S, Takagi Y, Tabata MJ, Hattori A (2005) Osteoblastic activity and estrogenic response in the regenerating scale of goldfish, a good model for osteogenesis. Life Sci 76:2699–2709